

# Convolution with even-sized kernels and symmetric padding

Shuang Wu<sup>1 2</sup> Guanrui Wang<sup>1 2</sup> Pei Tang<sup>1 2</sup> Feng Chen<sup>3 2</sup> Luping Shi<sup>1 2</sup>

## Abstract

Compact convolutional neural networks gain efficiency mainly through depthwise convolutions, expanded channels and complex topologies, which contrarily aggravate the training efforts. In this work, we identify the shift problem occurs in even-sized kernel ( $2 \times 2$ ,  $4 \times 4$ ) convolutions, and eliminate it by proposing symmetric padding on each side of the feature maps (C2sp, C4sp). Symmetric padding enlarges the receptive fields of even-sized kernels with little computational cost. In classification tasks, C2sp outperforms the conventional  $3 \times 3$  convolution and obtains comparable accuracies to existing compact convolution blocks, but consumes less memory and time during training. In generation tasks, C2sp and C4sp both achieve improved image qualities and stabilized training. Symmetric padding coupled with even-sized convolution is easy to be implemented into deep learning frameworks, providing promising building units for architecture designs that emphasize training efforts on online and continual learning occasions.

## 1. Introduction

Deep convolutional neural networks (CNNs) have achieved significant successes in numerous computer vision tasks such as image classification (Simonyan & Zisserman, 2015), object detection (Girshick et al., 2014), medical image analysis (Esteva et al., 2017), and Atari games (Mnih et al., 2015). Other than domain-specific applications, various architectures have been designed to improve the performance of CNNs (He et al., 2016; Huang et al., 2017), wherein the feature extraction and representation capabilities are mostly enhanced by deeper and wider models containing ever-growing numbers of parameters and operations. Thus,

<sup>1</sup>Department of Precision Instrument, Tsinghua University, Beijing, China <sup>2</sup>Center for Brain Inspired Computing Research, Beijing Innovation Center for Future Chip, Beijing, China <sup>3</sup>Department of Automation, Tsinghua University, Beijing, China. Correspondence to: Luping Shi <lpshi@mail.tsinghua.edu.cn>, Feng Chen <chenfeng@mail.tsinghua.edu.cn>.

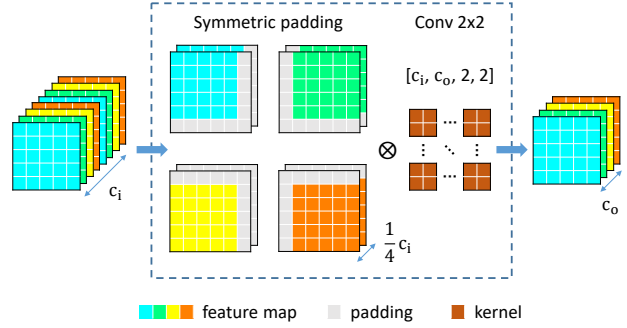


Figure 1. A naive implementation of convolution with  $2 \times 2$  kernels and symmetric padding (C2sp).  $c_i$  and  $c_o$  denote the number of input and output feature maps, respectively.  $c_i$  is an integer multiple of 4. Input feature maps are first divided equally into four groups, padded with zeros according to the direction defined in that group, and then convolved with even-sized kernels.

the memory overhead and computational complexity greatly impede their deployment in embedded AI systems with limited resources. This motivates the deep learning community to design compact CNNs and reduce hardware requirements, while still maintaining satisfactory performance.

Compact CNNs derive generalization capabilities from a variety of aspects. From the perspective of spatial correlation, the convolution with larger kernels tends to be factorized into a stack of smaller ones (Simonyan & Zisserman, 2015), efficiently approximating the same receptive fields (RFs). Irregular kernels enlarge RFs by dilations (Yu & Koltun, 2016) or adaptive deformations (Dai et al., 2017). Spatial convolution can also be achieved by moving feature maps (FMs) into different directions (Wu et al., 2017). From the perspective of channel correlation, FMs are expanded by pointwise convolution, group convolution (Xie et al., 2017), and bottleneck architecture (He et al., 2016). Depthwise-separable (Chollet, 2017) convolution decouples and separately realizes the spatial and channel correlations. Aside from human priors and handcrafted designs, emerging neural architecture search (NAS) methods optimize compact CNNs by reinforcement learning (Zoph et al., 2017) and evolution algorithm (Real et al., 2018).

Although many progresses have been made, most of them

only concentrate on the inference efforts judged by imperfect criteria: numbers of parameters and FLOPs. Whereas the training efforts are neglected or even becoming more intractable due to complex topologies (Liu et al., 2017), expanded channels (Sandler et al., 2018), as well as numerous operations and transformations that are not counted in the criteria, e.g., pooling, channel shuffle (Ma et al., 2018), FM shift (Wu et al., 2017), and batch normalization (Ioffe & Szegedy, 2015). With the growing demands for online and continual learning applications (Wu et al., 2018), the training efforts should be jointly addressed and further emphasized. Besides, recent advances in data augmentation (Zhang et al., 2017; DeVries & Taylor, 2017) have shown much powerful and universal benefits. Combining these methods easily eclipse the progresses made by intricate architecture engineering, inspiring us to return to simpler structures.

In this work, we balance the training and inference efforts, and focus on simple but efficient compact CNNs. We explore the generalization capabilities of even-sized kernels ( $2\times 2$ ,  $4\times 4$ ) that are deemed to be inferior to the widely-adopted  $3\times 3$  kernel. The performance degradation is mainly caused by the asymmetric padding inevitably occurs in even-sized kernels, which leads to 0.5 pixel shifts in the resulting FMs. The location offset accumulates when stacking multiple layers of even-sized convolutions, and eventually distorts the spatial information. To this end, we propose convolution with even-sized kernels and symmetric padding on each side of the feature maps (C2sp, C4sp).

As illustrated in Figure 1, the symmetric padding is computationally light and easy to incorporate into even-sized convolutions. It not merely eliminates the shift problem, but also extends receptive fields of even-sized kernels. Various classification results demonstrate that C2sp is an effective decomposition of C3 in terms of 30%-50% saving of parameters and FLOPs. Compared with other compact CNN blocks such as ShiftNet (Wu et al., 2017), inverted-bottleneck (Sandler et al., 2018) and depthwise-separable convolution (Chollet, 2017), C2sp achieves comparable performance with less memory consumption (>35%) and speeds up the training process (>20%). In generative adversarial networks (GANs) (Goodfellow et al., 2014), C2sp and C4sp both obtain improved image qualities and stabilized training. Our method provides promising building units for architecture designs that emphasize training efforts on online and continual learning occasions.

## 2. Related work

**Even-sized kernel** Since even-sized kernels are integer multiples of 2, they are mostly applied together with stride 2 to rescale images, which can avoid the checkerboard artifact (Odena et al., 2016). For example, the shallower models of

(Miyato et al., 2018) use  $4\times 4$  kernels and stride 2 in the discriminators and generators to down-sample and up-sample images. However,  $3\times 3$  kernel is mostly preferred when it comes to deep and large-scale GANs (Gulrajani et al., 2017; Karras et al., 2017; Kurach et al., 2018). In segmentation tasks, U-Net (Ronneberger et al., 2015) and its followers use  $2\times 2$  kernels to up-sample images. Except for scaling, very few works have implemented even-sized kernels as basic building blocks for their CNN models. In relational reinforcement learning (Zambaldi et al., 2018), two C2 layers are adopted to achieve reasoning and planning of objects represented by 4 pixels. It is discussed that factorizing a C3 into two C2s only provides 11% saving of overheads (Szegedy et al., 2016), but the performance is not evaluated.

**Shift kernel and feature map** In (Zhao et al., 2017), the authors randomly shift  $3\times 3$  kernels in the down-sampling layers (strided convolution or pooling) to reduce information loss. It can be viewed as a feature augmentation method applied during training. ShiftNet (Wu et al., 2017) sidesteps spatial convolutions entirely by using shift operations followed with pointwise convolutions. Though shift kernels contain no parameter or FLOP, ShiftNet expands too many FMs and is not such efficient regarding their evaluations. Deformable convolution (Dai et al., 2017) augments the spatial sampling locations of kernels by additional 2D offsets, and learning the offsets directly from the target tasks. Therefore, deformable kernels shift at pixel level and are more focused on geometric transformations.

**depthwise convolution** Depthwise convolution (DWConv) is an extreme case of group convolution in which the number of groups is equal to the number of channels. In practice, DWConv is usually coupled with a pointwise convolution, named as the depthwise-separable convolution (Chollet, 2017). The fundamental hypothesis behind is that the spatial and channel correlations can be sufficiently decoupled and separately realized. The overheads of DWConv is only linear to the channel number, so an inverted-bottleneck (Sandler et al., 2018) further improves the accuracy by expanding channels. Now DWConv and its extensions have become popular components for compact CNNs (Ma et al., 2018; Zoph et al., 2017; Real et al., 2018).

## 3. Symmetric padding

### 3.1. The shift problem

To explore compact CNNs with simple architecture, we start with the spatial correlation in basic convolution kernel size. Intuitively, replacing a C3 with two C2s should provide performance gains aside from 11% reduction of overheads, which is inspired by the factorization of C5 into two C3s (Simonyan & Zisserman, 2015). However, the experiments in Figure 4 indicate that the classification accuracies of C2 is

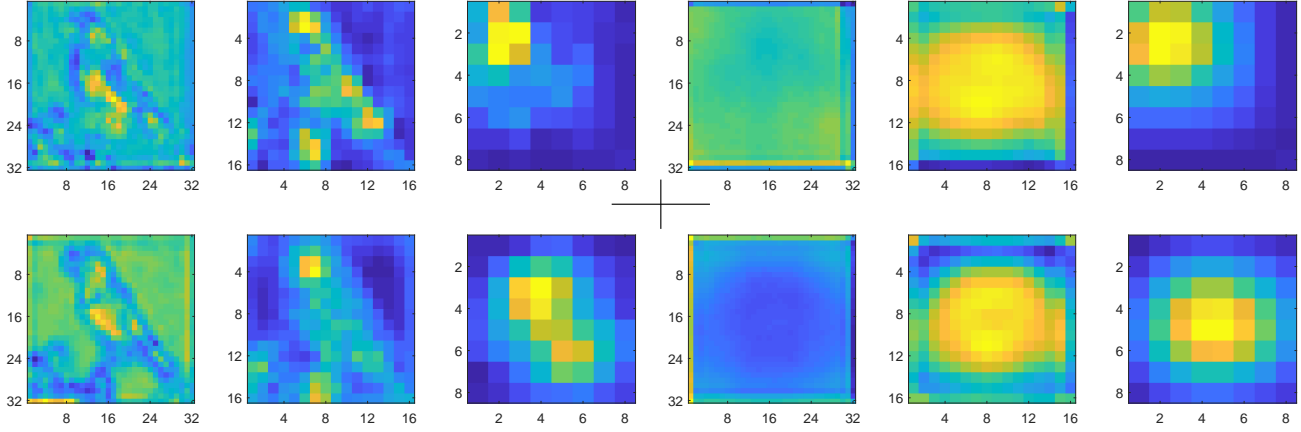


Figure 2. Feature maps derived from well-trained ResNet-56 models. Three spatial sizes  $32 \times 32$ ,  $16 \times 16$ , and  $8 \times 8$  before three down-sampling stages are presented. First row: Conv $2 \times 2$  with asymmetric padding (C2). Second row: Conv $2 \times 2$  with symmetric padding (C2sp). Left: a sample in CIFAR10 test dataset. Right: average results from all the samples in the test dataset.

inferior to C3 and saturate much faster as the network deepens. In addition, changing C3 to C4 also hurts accuracies even though the latter contains about 77% more parameters and FLOPs, and  $3 \times 3$  kernel can be regarded as a subset of  $4 \times 4$  kernel. To address this issue, the FMs of trained ResNet-56 models with  $2 \times 2$  kernels are shown in Figure 2. It is clearly seen that the post-activation (ReLU) values in C2 are gradually shifting to the left-top corner of the spatial location. FMs of  $4 \times 4$  kernels have the similar manner and are omitted for clarity. These compressed and distorted features are not suitable for the following classification, let alone pixel-level tasks based on it such as detection and semantic segmentation, where all the annotations will have offsets starting from the top-left corner of the image.

We identify this as the *shift problem* observed in even-sized kernels, for a conventional convolution between  $c_i$  input and  $c_o$  output FMs  $\mathcal{F}$  and square kernels of size  $k \times k$ , it can be described as

$$\mathcal{F}_o(\mathbf{p}) = \sum_{i=1}^{c_i} \sum_{\delta \in \mathcal{R}} \mathbf{w}_i(\delta) \cdot \mathcal{F}_i(\mathbf{p} + \delta), \quad (1)$$

where  $\delta$  and  $\mathbf{p}$  enumerate the locations in receptive field  $\mathcal{R}$  and in FMs of size  $h \times w$ , respectively. When  $k$  is an odd number, e.g., 3, we have

$$\begin{aligned} \mathcal{R} &= \{(-\kappa, -\kappa), (-\kappa, 1 - \kappa), \dots, (\kappa, \kappa)\}, \\ \kappa &= \lceil \frac{k-1}{2} \rceil, \end{aligned} \quad (2)$$

where  $\kappa$  denotes the calculated maximum pixel numbers for four sides of the receptive field.  $\lceil \cdot \rceil$  is the ceil rounding function. Since  $\mathcal{R}$  is symmetrical, we have

$$\sum_{\delta \in \mathcal{R}} \delta = (0, 0). \quad (3)$$

When  $k$  is an even number, e.g., 2 or 4, implementing convolution between  $\mathcal{F}_i$  and kernels  $\mathbf{w}$  becomes inevitably asymmetric since there is no “center pixel” to align. In most deep learning frameworks, this issue draws little attention and is obscured by pre-defined offsets. For example, `tf.nn.conv2d` in TensorFlow (Abadi et al., 2016) picks a nearest pixel in the left and top direction as the origin:

$$\mathcal{R} = \{(1 - \kappa, 1 - \kappa), (1 - \kappa, 2 - \kappa), \dots, (\kappa, \kappa)\}, \quad (4)$$

which leads to a shift in the accumulated  $\mathcal{R}$ :

$$\sum_{\delta \in \mathcal{R}} \delta = (1, 1). \quad (5)$$

The shift occurs at all the spatial locations of  $\mathbf{x}$  and is equivalent to pad one more zero on the bottom and right sides of FMs before convolutions. On the contrary, Caffe (Jia et al., 2014) pads one more zero on the left and top sides. PyTorch (Paszke et al., 2017) only supports symmetric padding by default, users need to manually and explicitly define the padding policy if desired.

According to the above, even-sized kernels make the zero-padding asymmetric with 1 pixel, and averagely (between two opposite directions) lead to 0.5 pixel shifts in the resulting FMs. The position offset accumulates when stacking multiple layers of even-sized convolutions, and eventually squeezes and distorts features to a certain corner of the spatial location. Ideally, in case that such asymmetric padding is performed for  $n$  times in the TensorFlow style with convolutions in between, the resulting pixel-to-pixel correspondence of FMs will be

$$\mathcal{F}_n[\mathbf{p} - (0.5n, 0.5n)] \leftarrow \mathcal{F}_0(\mathbf{p}). \quad (6)$$

It will not cause anything wrong if the image has infinite or large enough width and height. However, CNNs are usually

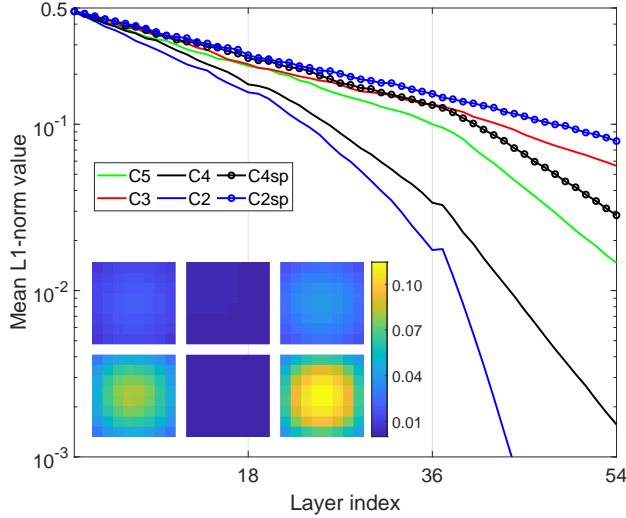


Figure 3. The layerwise  $Q$  in untrained ResNet-56 models and colormaps derived from the last convolution layers. FMs are down-sampled after layer indexes 18 and 36.

equipped with down-sampling layers to force high-level feature representations and reduce computational overheads. Then the *edge effect* (McGibney et al., 1993; Aghdasi & Ward, 1996) can not be ignored because zero-padding at edges will distort the effective values of FM, especially in deep networks and small feature maps. For an FM of size  $h \times w$ , we hypothesize that the quantity of information  $Q$  equals to the mean L1-norm value of the FM, then successive convolutions with zero-padding at four edges will gradually erase the information:

$$Q_n = \frac{1}{hw} \sum_{\mathbf{p} \in h \times w} |\mathcal{F}_n(\mathbf{p})| < Q_{n-1}. \quad (7)$$

Since the erosion happens recursively and is very complex to be formulated, we directly simulate FMs from untrained deep networks. In Figure 3, 10k images of size  $32 \times 32$  are fed into ResNet-56 models to get layerwise  $Q$  values. The identity connections and batch normalizations are removed to avoid the additional scaling. For each kernel size, the average result of 10 runs is reported. Regretfully,  $Q$  decreases progressively even though the values of parameters are initialized with MSRA method (He et al., 2015). The corrosion happens faster in larger kernel sizes and smaller FMs. Besides, asymmetric padding speeds up the process in even-sized kernels dramatically, which is in consistent with the results of well-trained networks in Figure 2.

An analogy is that FM can be seen as a rectangular ice chip melting in the water except that it can only exchange heat on its four edges. The smaller the ice, the faster the melting process happens. Asymmetric padding produces larger thermal gradients on certain edges, thus accelerating the

exchange. Whereas symmetric padding equally distributes thermal gradients so as to slow it down. It also provides possible explanation for the degradation problem in very deep networks (He et al., 2016), where forward activations and backward gradients exhibit healthy  $Q$  with batch normalization. Although the magnitude of  $Q$  is normalized, the spatial information is blurred by the edge effect after multiple convolution layers, as well as distorted by the shift problem in even-sized kernels.

### 3.2. Method

To introduce symmetry, it is difficult to transform the Equation 5 directly into Equation 3 since  $\mathcal{R}$  is inevitably asymmetric for even kernels. Instead, we aim at the final output  $\mathcal{F}_o$  which are summed by  $c_i$  input  $\mathcal{F}_i$  and kernels. For clarity, let  $\mathcal{R}(1, 1)$  be the asymmetric pattern in Equation 4 that produces shift in the left and top direction, then we explicitly produce a shift collection including four directions:

$$\mathcal{R}_+ = \{\mathcal{R}(1, 1), \mathcal{R}(-1, 1), \mathcal{R}(1, -1), \mathcal{R}(-1, -1)\}, \quad (8)$$

such that

$$\sum_{i=1}^{c_i} \sum_{\delta \in \mathcal{R}_+} \delta = (0, 0). \quad (9)$$

A straightforward solution is to randomly define  $\mathcal{R}$  for  $c_i$  FMs when initializing each convolution in CNN models, and maintain the same shift patterns during training. Equivalently, if  $c_i$  is an integer multiple of 4, the symmetry is strictly obeyed by dividing and defining convolution equally into four groups:

$$\mathcal{F}_o(\mathbf{p}) = \sum_{i=1}^{c_i} \sum_{\delta \in \mathcal{R}_+ \setminus \{4i/c_i\}} \mathbf{w}_i(\delta) \cdot \mathcal{F}_i(\mathbf{p} + \delta). \quad (10)$$

This convolution can be efficiently realized by a slight change of the padding strategy, which is also illustrated in Figure 1. In summary, the 2D convolution with even-sized kernels and symmetric padding consists of two steps: (1) Padding FMs in a symmetric style. It can be viewed as a special case of shift operation or deformable convolution, that only shifts a single step for the whole FM. (2) Calculating summation of sampled values weighted by even-sized kernels  $\mathbf{w}$ . It is exactly the same arithmetic as conventional convolution without paddings.

## 4. Experiments

In this section, the efficacy of symmetric padding is validated in CIFAR (Krizhevsky & Hinton, 2009) and ImageNet (Russakovsky et al., 2015) classification tasks, as well as CIFAR, LSUN bedroom (Yu et al., 2015), and CelebA-HQ (Karras et al., 2017) generation tasks. In classifications, we focus on C2sp since it is more efficient than C3. Whereas in



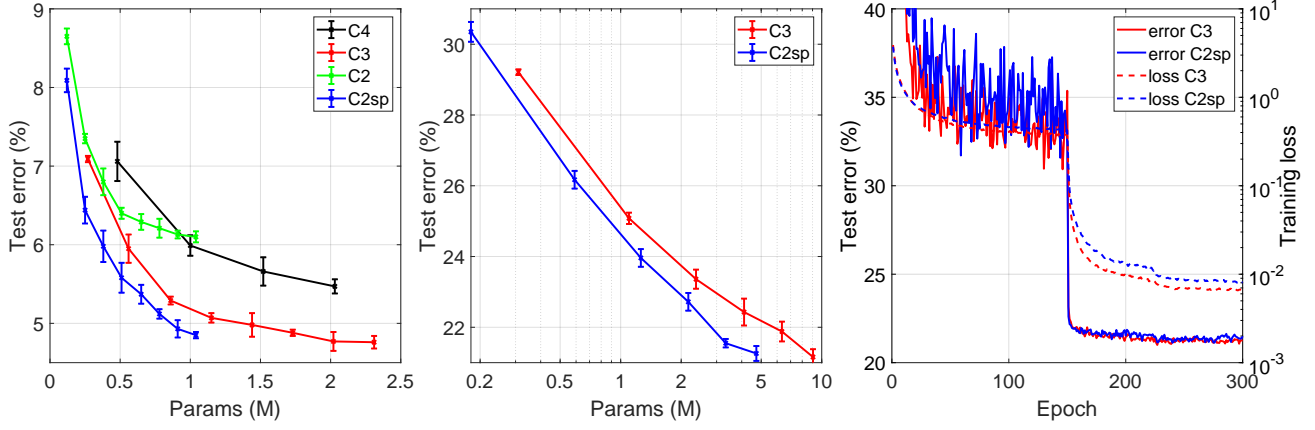


Figure 4. Left: comparison of the parameter efficiency on ResNets that have multiple depths and various convolution kernels. Middle: comparison of the parameter efficiency between C3 and C2sp on DenseNets that have multiple depths. Right: training and testing curves on DenseNet-112 with C3 and C2sp.

image generation with GANs, C2sp and C4sp both achieve improved image qualities and stabilized training. The implementation and training details are described in Section 4.5.

First of all, we check whether the shift problem has been eliminated by symmetric padding. Feature maps derived from well-trained ResNet-56 models with C2 or C2sp are shown in Figure 2. In the original asymmetric case, the perceptual features already have obvious position shift in  $16 \times 16$  FMs, and are later squeezed to the left and top corner in the  $8 \times 8$  spatial locations. Therefore, the high-level representations are compressed and distorted in much smaller response fields. Without increasing any parameter or computation, our proposed symmetric padding method not only eliminates the shift problem, but also broadens the receptive fields of even-sized kernels and alleviates the edge effect. The layerwise  $\mathcal{Q}$  values in untrained models are shown in Figure 3. Compared with C2 and C4, C2sp and C4sp have much lower attenuation rates. C2sp has larger  $\mathcal{Q}$  than C3, expecting performance growth in the following evaluations.

#### 4.1. Convolutions with various kernel sizes

To validate the efficiency of C2sp and other convolution kernels, ResNet series without bottleneck architectures (He et al., 2016) are chosen as the backbones. We maintain all the other components and training hyperparameters as the same, and only replace the original C3 by C4, C2 or C2sp. The networks are trained on CIFAR10 dataset with depth varies in  $6n + 2$ ,  $n \in \{3, 6, \dots, 24\}$ . The parameter-accuracy curves are shown in Figure 4. The original even-sized kernels  $4 \times 4$ ,  $2 \times 2$  perform poorly and encounter faster saturation as the network deepens. Compared with C3, C2sp reaches the same accuracies with only 60%-70% of the parameters, as well as FLOPs that are linearly correlated. We also find that symmetric padding only slightly improves the

accuracies in C4sp. In such network depth, the edge effect might dominate the degradation of  $4 \times 4$  kernels, which is consistent with attenuation curves in Figure 3.

Based on the results of ResNets on CIFAR10, we further compare C2sp and C3 on CIFAR100 dataset. At this time, DenseNet (Huang et al., 2017) series with multiple depths in  $6n + 4$ ,  $n \in \{3, 6, \dots, 18\}$  are the backbones, and the results are shown in Figure 4. At the same depth, C2sp achieves comparable accuracies as the network gets deeper. The training losses indicate that C2sp have better generalization and less overfitting than C3. Although it is discussed that factorizing a C3 into two C2s only provides 11% saving of overheads, the performance growth amplifies the saving to about 30%-50% under the same accuracies in CIFAR10 and CIFAR100 evaluations. Therefore, we recommend using C2sp as a better alternative to C3 in classifications.

#### 4.2. Compare with efficient convolutions

To facilitate fair comparisons for C2sp with other efficient building blocks that contain pointwise convolutions, DW-Convs, or shift kernels, we use ResNets as backbones and adjust widths and depths of the models to maintain the same amount of overheads. In case there are  $n$  input channels for a building block, then a two-layer residual block with C2sp will consume about  $8n^2$  parameters and FLOPs. The expansion is marked as 1-1-1 since no channel expansion happens. For ShiftNet blocks (Wu et al., 2017), we choose the expansion rate 3 and  $3 \times 3$  shift kernels, the overheads are about  $6n^2$ . Therefore, the number of blocks remains the same but the value of  $n$  is slightly increased. While for the inverted-bottleneck (Sandler et al., 2018), the expansion rate equals to 6 as suggested by the authors. This huge expansion results in  $12n^2 + O(6n)$  overheads, thus we reduce the number of blocks by  $\frac{1}{3}$ . For depthwise-separable convolutions

Table 1. Comparison on CIFAR100 dataset. Shift, Invert, and Sep denote ShiftNet block, inverted-bottleneck, and depthwise-separable convolution, respectively. *mixup* denotes training with mixup augmentation, and Expand denotes the expansion rates of channels in building blocks.

Model	Block	Error (%)		Param (M)	Complexity (MFLOPs)	Expand	Memory (MB)	Speed (FPS)
		standard	with <i>mixup</i>					
20	Shift	26.87 $\pm$ 0.19	24.74 $\pm$ 0.04	0.49	70.0	1-3-1	853	1906
	Invert	26.86 $\pm$ 0.11	25.32 $\pm$ 0.12	0.42	76.7	1-6-1	1219	2057
	Sep	26.70 $\pm$ 0.20	<b>23.81 <math>\pm</math> 0.15</b>	0.51	73.6	2-2-2	732	2709
	C2sp	26.77 $\pm$ 0.19	24.90 $\pm$ 0.17	0.50	73.2	1-1-1	<b>487</b>	<b>3328</b>
56	Shift	24.07 $\pm$ 0.24	21.31 $\pm$ 0.21	1.48	213.4	1-3-1	2195	683
	Invert	<b>22.36 <math>\pm</math> 0.25</b>	21.48 $\pm$ 0.25	1.52	240.1	1-6-1	2561	803
	Sep	23.31 $\pm$ 0.09	<b>20.69 <math>\pm</math> 0.11</b>	1.47	218.0	2-2-2	1707	1034
	C2sp	23.19 $\pm$ 0.29	20.91 $\pm$ 0.22	1.54	224.2	1-1-1	<b>1219</b>	<b>1230</b>
110	Shift	22.94 $\pm$ 0.26	20.47 $\pm$ 0.18	2.97	428.3	1-3-1	4146	348
	Invert	<b>21.76 <math>\pm</math> 0.17</b>	20.43 $\pm$ 0.20	3.17	485.1	1-6-1	4756	426
	Sep	22.31 $\pm$ 0.22	<b>19.42 <math>\pm</math> 0.05</b>	2.91	434.4	2-2-2	3170	540
	C2sp	21.93 $\pm$ 0.04	19.52 $\pm$ 0.10	3.10	450.7	1-1-1	<b>1951</b>	<b>636</b>

(Chollet, 2017), the overheads are about  $2n^2 + O(n)$ , so the channels are doubled and formed as 2-2-2 expansions.

The results are summarized in Table 1. Most models easily overfit the CIFAR100 training set. So aside from the standard augmentation, we also train the models with mixup (Zhang et al., 2017) augmentation to fully release their generalization capabilities, and make the differences more significant. In addition to error rates, the memory consumption and speed during training are reported. C2sp performs better accuracies than ShiftNets, which indicates that sidestepping spatial convolutions entirely by shift operations may not be an efficient solution. Compared with blocks that contain DWConv, C2sp achieves comparable results in 56 and 110 nets with fewer channels and simpler architectures, which reduce memory consumption ( $>35\%$ ) and speed up ( $>20\%$ ) the training process.

Table 2. Test error rates (%) on CIFAR10 dataset. c/o and *mixup* denotes cutout and mixup data augmentation.

Model	Error (%)	Param (M)
NASNet-A (Zoph et al., 2017)	3.41	3.3
PNASNet-5 (Liu et al., 2017)	3.41	3.2
AmoebaNet-A (Real et al., 2018)	<b>3.34</b>	3.2
Wide-DenseNet C2sp	3.54	3.2
NASNet-A + c/o (Zoph et al., 2017)	2.65	3.3
Wide-DenseNet C2sp + c/o + <i>mixup</i>	<b>2.44</b>	3.2

In Table 2, we compare C2sp with NAS models: NASNet (Zoph et al., 2017), PNASNet (Liu et al., 2017)

and AmoebaNet (Real et al., 2018). We apply Wide-DenseNet (Huang et al., 2017) and adjust the width and depth ( $K = 48, L = 50$ ) to have approximately 3M parameters. C2sp only suffers less than 0.2% accuracy loss compared with state-of-the-art generated models, and achieves a better accuracy when the augmentation is enhanced. Despite that NAS models have similar numbers of parameters, the training speeds on TitanXP for Wide-DenseNet and NASNet-A are about 400 and 200 FPS, respectively. The reason is that NAS models mostly contain lots of small fragmented operators (Ma et al., 2018) rather than a few large ones. Although these small operators, e.g., pooling, group convolution, DWConv, show improvements in accuracy with less computation cost, they also make the network more fragmented and limit the use of hardware resources in parallel. Thus, the regular-structured Wide-DenseNet has better computational efficiency in runtime.

### 4.3. ImageNet classification

We start with the widely-used ResNet-50 and DenseNet-121 models. Since both of them contain bottlenecks and pointwise convolutions to scale down the number of channels,  $3 \times 3$  convolutions only consume about 53% and 32% of the total overheads. Changing the  $3 \times 3$  kernels to  $2 \times 2$  then results in about 25% and 17% reduction of parameters and FLOPs, respectively. The top-1 classification accuracies are shown in Table 3, C2sp have minor loss (0.2%) in ResNet, and suffers slightly larger degradation (0.5%) in DenseNet. After all, there are only 0.9M parameters for spatial convolution in DenseNet-121 C2sp.

We further scale the channels of ResNet-50 down to  $0.5 \times$  as a mobile setting. At this stage, an asymmetric C2 model, as

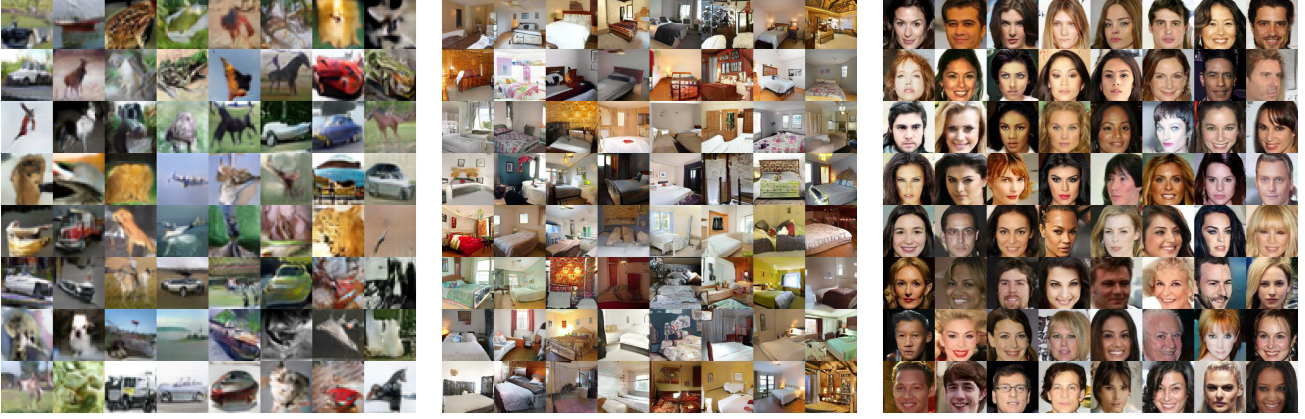


Figure 5. Examples generated by GANs on CIFAR10 ( $32 \times 32$ , C2sp, Inception Score = 8.27, FID=19.49), LSUN-bedroom ( $128 \times 128$ , C4sp, FID=16.63) and CelebA-HQ ( $128 \times 128$ , C4sp, FID=19.83) dataset.

Table 3. Top-1 error rates on ImageNet. Results are obtained by our reproductions using the same hyperparameters.

Model	Error (%)	Param (M)
ResNet-50 C3 (He et al., 2016)	<b>23.8</b>	25.5
ResNet-50 C2sp	24.0	19.3
DenseNet-121 C3 (Huang et al., 2017)	24.6	8.0
DenseNet-121 C2sp	25.1	<b>6.7</b>
ResNet-50 $0.5 \times$ C3	27.9	6.9
ResNet-50 $0.5 \times$ C2	30.9	5.3
ResNet-50 $0.5 \times$ C2sp	28.4	<b>5.3</b>
MobileNet v2 $1.4 \times$ (Sandler et al., 2018)	<b>25.8</b>	6.1
ShuffleNet v2 $2.0 \times$ (Ma et al., 2018)	27.5	7.4
MobileNet v2 $1.0 \times$ (Sandler et al., 2018)	28.7	3.5
ShuffleNet v2 $1.5 \times$ (Ma et al., 2018)	29.3	3.5

well as reproductions of MobileNet-v2 (Sandler et al., 2018) and ShuffleNet-v2 (Ma et al., 2018) are evaluated. Symmetric padding reduces the error rate of ResNet-50  $0.5 \times$  C2 for 2.5%, making the mediocre ResNet a comparable solution to compact CNNs. Although MobileNet-v2 models achieve the best accuracies, they use pointwise convolution to expand too many feature maps (the same inverted-bottleneck in Table 1), which significantly increase the memory consumption and training time for training (about 400 FPS), while other models can easily reach 1000 FPS. All the models are trained with nearly the same hyperparameters for fair comparisons. Therefore, some results are worse than reported in the original papers. It is likely due to the inconsistency of mini-batch size, learning rate decay, or total training epochs, e.g., about 420 epochs in (Sandler et al., 2018).

#### 4.4. Image generation

The efficacy of symmetric padding is further validated in image generation tasks with GANs. Two classes of residual networks are explored on three datasets. In CIFAR10  $32 \times 32$  image generation, we follow the same ResNet architecture described in (Miyato et al., 2018), which has about 6M parameters in the generator and 1.5M parameters in the discriminator. In LSUN bedroom and CelebA-HQ  $128 \times 128$  image generations, ResNet19 (Kurach et al., 2018) is adopted with five residual blocks in the generator and six residual blocks in the discriminator, containing about 14M parameters for each of them. Since the training of GAN is a zero-sum game between two neural networks, to mitigate the influences cause by other factors, we remain all discriminators as the same, and replace the C3 in generators with C4, C2, C4sp, and C2sp. Besides, the number of channels are reduced to  $0.75 \times$  in C4 and C4sp, or expanded  $1.5 \times$  in C2 and C2sp to approximate the same number of parameters for generators.

Table 4. Scores for different kernels. Top: CIFAR10  $32 \times 32$  inception scores and FIDs. Bottom: LSUN bedroom and CelebA-HQ  $128 \times 128$  FIDs. Higher inception score and lower FID is better.

Kernel	Inception Score	FID
C4	$7.76 \pm 0.11$	$26.45 \pm 1.50$
C3	$7.79 \pm 0.06$	$24.12 \pm 0.47$
C4sp	$7.74 \pm 0.08$	$24.86 \pm 0.41$
C2sp	$7.77 \pm 0.05$	<b><math>23.35 \pm 0.26</math></b>
Kernel	LSUN bedroom	CelebA-HQ
C4	$39.17 \pm 5.52$	$37.93 \pm 7.54$
C3	$36.04 \pm 7.10$	$43.39 \pm 5.78$
C4sp	<b><math>24.61 \pm 2.45</math></b>	<b><math>30.22 \pm 3.02</math></b>
C2sp	$27.73 \pm 6.76$	$31.25 \pm 4.86$



The inception scores (Salimans et al., 2016) and FIDs (Heusel et al., 2017) are shown in Table 4 for quantitatively evaluating generated images, and examples from the best FID runs are visualized in Figure 5. Without symmetric padding, C2 generators can not converge in our experiments. On CIFAR10 dataset, C2sp performs the best scores and symmetric padding improves the image quality of C4 as well. While in LSUN bedroom and CelebA-HQ generations, C4sp is slightly better than C2sp because the network depth is relatively shallow in terms of  $128 \times 128$  image size, and the edge effect is negligible. Then larger receptive fields might be more important than wider channels in high resolution image generations. In addition, the standard derivations of inception scores and FIDs confirm that symmetric padding stabilize the training of GANs.

#### 4.5. Training details

Results reported as mean $\pm$ std in tables or error bars in figures are trained for 5 times with different random seeds. The default settings for CIFAR classifications are as follows: We train models for 300 epochs with mini-batch size 64 except for the results in Table 2, which run 600 epochs as in (Zoph et al., 2017). We use the cosine learning rate decay (Loshchilov & Hutter, 2016) starting from 0.1 except for DenseNet tests, where the piecewise constant decay performs better. The weight decay factor is  $1e-4$  except for parameters in depthwise convolutions. The standard augmentation (Lee et al., 2015) is applied and the  $\alpha$  equals to 1 in mixup augmentation. For ImageNet classifications, all the models are trained for 100 epochs with mini-batch size 256. Learning rate is set to 0.1 initially and annealed according to cosine decay schedule. We follow the data augmentation in (Silberman & Guadarrama, 2017). Weight decay is  $1e-4$  in ResNet-50 and DenseNet-121 models, and decreases to  $4e-5$  in the other compact models.

In generation tasks with GANs, we follow models and hyperparameters recommended in (Kurach et al., 2018). Learning rate is 0.2,  $\beta_1$  is 0.5 and  $\beta_2$  is 0.999 for Adam optimizer (Kingma & Ba, 2015). The batchsize is 64, the ratio of discriminator to generator updates is 5:1 ( $n_{\text{critic}} = 5$ ). The results in Table 4 and Figure 5 are trained for 200k and 500k discriminator update steps, respectively. We use the non-saturation loss (Goodfellow et al., 2014) without gradient norm penalty (Gulrajani et al., 2017). The spectral normalization (Miyato et al., 2018) is applied in discriminators, no normalization is applied in generators.

## 5. Discussion

From the evaluations above, C2sp achieves comparable accuracies with less training memory and time. Although fragmented operators distributed in many groups have fewer parameters and FLOPs, the *operational intensity* (Williams

et al., 2009) decreases as the group number increases. This negatively impacts the efficiency of computation, energy, and bandwidth in hardware that has strong parallel computing capabilities. In the situation where memory access dominates the computation, e.g., training, the reduction in FLOPs will be less meaningful. We can conclude that it is still controversial to decompose spatial and channel correlations completely by using DWConvs, shift operations, and pointwise convolutions, especially when the training efforts are emphasized.

Meanwhile, most deep learning frameworks and hardware are mainly optimized for C3, which restrains the efficiency of C2sp to some extent. In our high-level python implementation in TensorFlow for models with C2sp, C2 and C3, despite that the parameters and FLOPs ratio is 4:4:9, the speed and memory ratio during training is about 1:1.14:1.2 and 1:0.7:0.7. It is obvious that the speed and memory overheads for C2sp can be further optimized by basic computation libraries such as cuDNN.

## 6. Conclusion

In this work, we introduce symmetric padding to eliminate the shift problem occurs in even-sized kernels. Symmetric padding enlarges the receptive fields of even-sized kernels without increasing any parameter or computation. In classifications, C2sp achieves 30%-50% saving of parameters and FLOPs compared to C3 on CIFAR dataset, and have minor accuracy loss in widely-used models for ImageNet. Compared to existing compact convolution blocks, C2sp achieves comparable results with fewer channels and simpler architectures, which reduce memory consumption ( $>35\%$ ) and speed up ( $>20\%$ ) the training process. In generation tasks, C2sp and C4sp both achieve improved image qualities and stabilized training. Even-sized kernels with symmetric padding provide promising building units for architecture designs that emphasize training efforts on online and continual learning occasions.

## References

- Abadi, M., Barham, P., Chen, J., Chen, Z., Davis, A., Dean, J., Devin, M., Ghemawat, S., Irving, G., Isard, M., et al. Tensorflow: a system for large-scale machine learning. In *OSDI*, volume 16, pp. 265–283, 2016.
- Aghdasi, F. and Ward, R. K. Reduction of boundary artifacts in image restoration. *IEEE Transactions on Image Processing*, 5(4):611–618, 1996.
- Chollet, F. Xception: Deep learning with depthwise separable convolutions. *arXiv preprint*, pp. 1610–02357, 2017.
- Dai, J., Qi, H., Xiong, Y., Li, Y., Zhang, G., Hu, H., and



- Wei, Y. Deformable convolutional networks. *CoRR*, *abs/1703.06211*, 1(2):3, 2017.
- DeVries, T. and Taylor, G. W. Improved regularization of convolutional neural networks with cutout. *arXiv preprint arXiv:1708.04552*, 2017.
- Esteva, A., Kuprel, B., Novoa, R. A., Ko, J., Swetter, S. M., Blau, H. M., and Thrun, S. Dermatologist-level classification of skin cancer with deep neural networks. *Nature*, 542(7639):115–118, 2017.
- Girshick, R., Donahue, J., Darrell, T., and Malik, J. Rich feature hierarchies for accurate object detection and semantic segmentation. In *Proceedings of the IEEE conference on computer vision and pattern recognition*, pp. 580–587, 2014.
- Goodfellow, I., Pouget-Abadie, J., Mirza, M., Xu, B., Warde-Farley, D., Ozair, S., Courville, A., and Bengio, Y. Generative adversarial nets. In *Advances in neural information processing systems*, pp. 2672–2680, 2014.
- Gulrajani, I., Ahmed, F., Arjovsky, M., Dumoulin, V., and Courville, A. C. Improved training of wasserstein gans. In *Advances in Neural Information Processing Systems*, pp. 5767–5777, 2017.
- He, K., Zhang, X., Ren, S., and Sun, J. Delving deep into rectifiers: Surpassing human-level performance on imagenet classification. In *Proceedings of the IEEE international conference on computer vision*, pp. 1026–1034, 2015.
- He, K., Zhang, X., Ren, S., and Sun, J. Deep residual learning for image recognition. In *Proceedings of the IEEE conference on computer vision and pattern recognition*, pp. 770–778, 2016.
- Heusel, M., Ramsauer, H., Unterthiner, T., Nessler, B., and Hochreiter, S. Gans trained by a two time-scale update rule converge to a local nash equilibrium. In *Advances in Neural Information Processing Systems*, pp. 6626–6637, 2017.
- Huang, G., Liu, Z., Van Der Maaten, L., and Weinberger, K. Q. Densely connected convolutional networks. In *CVPR*, volume 1, pp. 3, 2017.
- Ioffe, S. and Szegedy, C. Batch normalization: Accelerating deep network training by reducing internal covariate shift. In *International Conference on Machine Learning*, pp. 448–456, 2015.
- Jia, Y., Shelhamer, E., Donahue, J., Karayev, S., Long, J., Girshick, R., Guadarrama, S., and Darrell, T. Caffe: Convolutional architecture for fast feature embedding. In *Proceedings of the 22nd ACM international conference on Multimedia*, pp. 675–678. ACM, 2014.
- Karras, T., Aila, T., Laine, S., and Lehtinen, J. Progressive growing of gans for improved quality, stability, and variation. *arXiv preprint arXiv:1710.10196*, 2017.
- Kingma, D. P. and Ba, J. Adam: A method for stochastic optimization. *International Conference on Learning Representations*, 2015.
- Krizhevsky, A. and Hinton, G. Learning multiple layers of features from tiny images. 2009.
- Kurach, K., Lucic, M., Zhai, X., Michalski, M., and Gelly, S. The gan landscape: Losses, architectures, regularization, and normalization. *arXiv preprint arXiv:1807.04720*, 2018.
- Lee, C.-Y., Xie, S., Gallagher, P., Zhang, Z., and Tu, Z. Deeply-supervised nets. In *Artificial Intelligence and Statistics*, pp. 562–570, 2015.
- Liu, C., Zoph, B., Shlens, J., Hua, W., Li, L.-J., Fei-Fei, L., Yuille, A., Huang, J., and Murphy, K. Progressive neural architecture search. *arXiv preprint arXiv:1712.00559*, 2017.
- Loshchilov, I. and Hutter, F. Sgdr: Stochastic gradient descent with warm restarts. *arXiv preprint arXiv:1608.03983*, 2016.
- Ma, N., Zhang, X., Zheng, H.-T., and Sun, J. Shufflenet v2: Practical guidelines for efficient cnn architecture design. In *Proceedings of the European Conference on Computer Vision (ECCV)*, pp. 116–131, 2018.
- McGibney, G., Smith, M., Nichols, S., and Crawley, A. Quantitative evaluation of several partial fourier reconstruction algorithms used in mri. *Magnetic resonance in medicine*, 30(1):51–59, 1993.
- Miyato, T., Kataoka, T., Koyama, M., and Yoshida, Y. Spectral normalization for generative adversarial networks. *International Conference on Learning Representations*, 2018.
- Mnih, V., Kavukcuoglu, K., Silver, D., Rusu, A. A., Veness, J., Bellemare, M. G., Graves, A., Riedmiller, M., Fidjeland, A. K., Ostrovski, G., et al. Human-level control through deep reinforcement learning. *Nature*, 518(7540): 529–533, 2015.
- Odena, A., Dumoulin, V., and Olah, C. Deconvolution and checkerboard artifacts. *Distill*, 1(10):e3, 2016.
- Paszke, A., Gross, S., Chintala, S., Chanan, G., Yang, E., DeVito, Z., Lin, Z., Desmaison, A., Antiga, L., and Lerer, A. Automatic differentiation in pytorch. In *NIPS-W*, 2017.

- Real, E., Aggarwal, A., Huang, Y., and Le, Q. V. Regularized evolution for image classifier architecture search. *arXiv preprint arXiv:1802.01548*, 2018.
- Ronneberger, O., Fischer, P., and Brox, T. U-net: Convolutional networks for biomedical image segmentation. In *International Conference on Medical image computing and computer-assisted intervention*, pp. 234–241. Springer, 2015.
- Russakovsky, O., Deng, J., Su, H., Krause, J., Satheesh, S., Ma, S., Huang, Z., Karpathy, A., Khosla, A., Bernstein, M., et al. Imagenet large scale visual recognition challenge. *International Journal of Computer Vision*, 115(3): 211–252, 2015.
- Salimans, T., Goodfellow, I., Zaremba, W., Cheung, V., Radford, A., and Chen, X. Improved techniques for training gans. In *Advances in Neural Information Processing Systems*, pp. 2234–2242, 2016.
- Sandler, M., Howard, A., Zhu, M., Zhmoginov, A., and Chen, L.-C. Mobilenetv2: Inverted residuals and linear bottlenecks. In *Proceedings of the IEEE Conference on Computer Vision and Pattern Recognition*, pp. 4510–4520, 2018.
- Silberman, N. and Guadarrama, S. Tensorflowslim image classification model library, 2017.
- Simonyan, K. and Zisserman, A. Very deep convolutional networks for large-scale image recognition. *International Conference on Learning Representations*, 2015.
- Szegedy, C., Vanhoucke, V., Ioffe, S., Shlens, J., and Wojna, Z. Rethinking the inception architecture for computer vision. In *Proceedings of the IEEE conference on computer vision and pattern recognition*, pp. 2818–2826, 2016.
- Williams, S., Waterman, A., and Patterson, D. Roofline: an insightful visual performance model for multicore architectures. *Communications of the ACM*, 52(4):65–76, 2009.
- Wu, B., Wan, A., Yue, X., Jin, P., Zhao, S., Golmant, N., Gholaminejad, A., Gonzalez, J., and Keutzer, K. Shift: A zero flop, zero parameter alternative to spatial convolutions. *arXiv preprint arXiv:1711.08141*, 2017.
- Wu, S., Li, G., Chen, F., and Shi, L. Training and inference with integers in deep neural networks. In *International Conference on Learning Representations*, 2018.
- Xie, S., Girshick, R., Dollár, P., Tu, Z., and He, K. Aggregated residual transformations for deep neural networks. In *Computer Vision and Pattern Recognition (CVPR), 2017 IEEE Conference on*, pp. 5987–5995. IEEE, 2017.
- Yu, F. and Koltun, V. Multi-scale context aggregation by dilated convolutions. 2016.
- Yu, F., Seff, A., Zhang, Y., Song, S., Funkhouser, T., and Xiao, J. Lsun: Construction of a large-scale image dataset using deep learning with humans in the loop. *arXiv preprint arXiv:1506.03365*, 2015.
- Zambaldi, V., Raposo, D., Santoro, A., Bapst, V., Li, Y., Babuschkin, I., Tuyls, K., Reichert, D., Lillicrap, T., Lockhart, E., et al. Relational deep reinforcement learning. *arXiv preprint arXiv:1806.01830*, 2018.
- Zhang, H., Cisse, M., Dauphin, Y. N., and Lopez-Paz, D. mixup: Beyond empirical risk minimization. *arXiv preprint arXiv:1710.09412*, 2017.
- Zhao, G., Wang, J., and Zhang, Z. Random shifting for cnn: a solution to reduce information loss in down-sampling layers. In *Proceedings of the 26th International Joint Conference on Artificial Intelligence*, pp. 3476–3482. AAAI Press, 2017.
- Zoph, B., Vasudevan, V., Shlens, J., and Le, Q. V. Learning transferable architectures for scalable image recognition. *arXiv preprint arXiv:1707.07012*, 2(6), 2017.